

Fast-evolving weather for the coolest of our two new substellar neighbours

M. Gillon¹, A. H. M. J. Triaud^{2,3}, E. Jehin¹, L. Delrez¹, C. Opitom¹, P. Magain¹, M. Lendl⁴, D. Queloz⁴

¹ Institut d'Astrophysique et Géophysique, Université de Liège, allée du 6 Août 17, B-4000 Liège, Belgium

² Department of Physics, and Kavli Institute for Astrophysics and Space Research, Massachusetts Institute of Technology, Cambridge, MA 02139, USA

³ Fellow of the Swiss National Science Foundation

⁴ Observatoire de Genève, Université de Genève, 51 Chemin des Maillettes, 1290 Sauverny, Switzerland

Received date / accepted date

ABSTRACT

We present the results of an intense photometric monitoring in the near-infrared ($\sim 0.9 \mu\text{m}$) with the TRAPPIST robotic telescope of the newly discovered binary brown dwarf WISE J104915.57-531906.1, the third closest system to the Sun at a distance of only 2 pc. Our twelve nights of photometric time-series reveal a quasi-periodic ($P = 4.87 \pm 0.01\text{h}$) variability with a maximal peak-peak amplitude of $\sim 11\%$ and strong night-to-night evolution. We attribute this variability to the rotational modulation of fast-evolving weather patterns in the atmosphere of the coolest component ($\sim \text{T1}$ -type) of the binary, in agreement with the cloud fragmentation mechanism proposed to drive the spectroscopic morphologies of brown dwarfs at the L/T transition. No periodic signal is detected for the hottest component ($\sim \text{L8}$ -type). For both brown dwarfs, our data allow us to firmly discard any unique transit during our observations for planets $\geq 2R_{\oplus}$. For orbital periods smaller than $\sim 9.5\text{h}$, transiting planets are excluded down to an Earth-size.

Key words. brown dwarfs – solar neighborhood – stars: individual: WISE-J104915.57-531906.1 – techniques: photometric

1. Introduction

Both inaugurated in 1995 (Rebolo et al. 1995; Mayor & Queloz 1995), the observational studies of brown dwarfs (BD) and exoplanets are two of the most active fields of modern astronomy. Notably, the atmospheric study of these substellar objects has seen tremendous advances recently, thanks to both the sophistication of models and the constant improvement of instruments (see, e.g., Seager & Deming 2010 and Showman & Kaspi 2012 for reviews). With their effective temperatures ranging from $\sim 300\text{--}2000\text{ K}$, L and T-types field BDs amenable for detailed direct studies represent critical precursors to the atmospheric characterization of giant planets spanning a wide range of age and irradiation. The data gathered so far for brown dwarfs outline the important role of atmospheric condensates on the spectral morphologies of these objects (Kirckpatrick 2005). This is especially true at the L-T transition ($\sim \text{L7-T4}$ spectral types) which is characterized by an increase of the J -band luminosity with decreasing temperature (Vrba et al. 2004), explained by the gradual depletion of silicates in the cooler atmospheres that results in increasingly patchy cloud covers and thus increasingly small condensate opacity. Still, the details of this transition remain poorly understood. The complexity of the plausible phenomena in play prevent simple 1D atmospheric models to reproduce properly the observations (e.g. Saumon & Marley 2008). One of the mechanism put forward to explain the condensate depletion involves the fragmentation of the clouds (Burgasser et al. 2002) driven by convection in the troposphere. This scenario predicts relatively large ($\sim 1\text{--}20\%$) photometric variability around $1\mu\text{m}$ on rotational timescales, driven by the constant formation, evolution and complex dynamics of cloud holes in the upper atmosphere.

Brown dwarfs being very rapid rotators (typically a few hours, Herbst et al. 2007), this variability due to evolving weather patterns should be observable within a few nights of photometric monitoring. Still, because of the extreme faintness in the optical at the L/T transition, only a handful of near-infrared (NIR) monitoring using medium-sized ground-based telescopes or space-based facilities could reach the photometric precisions required for effectively detecting these predicted semi-periodic variabilities (Clarke et al. 2008; Artigau et al. 2009; Radigan et al. 2012; Khandrika et al. 2013; Apai et al. 2013). Some of these results agree nicely with the cloud fragmentation hypothesis, but there is still no clear evidence that BDs at the L/T transition are more variable than the other BDs (Khandrika et al. 2013). More high-precision photometric monitoring of L/T transition BDs are thus highly desirable, also because they can provide other important insights into the physics of these substellar objects, notably on the spatial and temporal distribution of cloud structures, vertical thermal profiles, degrees of differential rotation, and on their age, their rotation period decreasing monotonically with time.

A unique opportunity for this domain came up recently with the detection by Luhman (2013, hereafter L13) of an extremely nearby binary BD at only $2.02 \pm 0.15\text{ pc}$. This system, WISE J104915.57-531906.1 (hereafter Luhman 16, following Mamajek 2013), is the third closest system to Earth, making it an exquisite target for high signal-to-noise ratio follow-up ($J = 10.7$, $K = 8.8$). With spectral types $\text{L8} \pm 1$ for Luhman 16A and $\text{T1} \pm 2$ for Luhman 16B (Kniazev et al. 2013, hereafter K13; see also Burgasser et al. 2013), both of its components lie within the L/T transition. This amazing system makes possible to study extrasolar weather in great details, and in particular to bring invaluable constraints on the importance of cloud fragmentation in the atmospheric physics of L/T transition BDs. In this context,

Send offprint requests to: michael.gillon@ulg.ac.be

it represents an invaluable target for high-precision time-series photometry, an interest further reinforced by the classification of the pair as a possible variable in WISE All-Sky Source Catalog (L13). This motivated us to perform an intensive photometric monitoring of the system in the NIR using the 60cm robotic telescope TRAPPIST. We observed Luhman 16 for twelve nights, reaching a typical precision $\sim 0.2\%$ per bin of 10 min, thanks to the relatively large brightness of the system. This high precision allowed us to detect a clear quasi-periodic variability combined with a fast evolution of the observed patterns that we attribute to the T-dwarf Luhman 16B.

The next section presents our TRAPPIST data and their reduction. Our analysis of the resulting photometric time-series is described in Sec. 3. Finally, we discuss briefly our results in Sec. 4.

2. Data description

We monitored WISE 1049-5319 for twelve nights between 2013 March 14 and 26 with the robotic 60cm telescope TRAPPIST (*TR*ansiting *Pl*anets and *Pl*anetes/*m*als *S*mall *T*elescope; Gillon et al. 2011, Jehin et al. 2011) located at ESO La Silla Observatory in the Atacama Desert, Chile. TRAPPIST is equipped with a thermoelectrically-cooled $2K \times 2K$ CCD having a pixel scale of $0.65''$ that translates into a $22' \times 22'$ field of view. The observations were obtained with an exposure time of 115s, with the telescope focused and through a special '*I* + *z*' filter having a transmittance $>90\%$ from 750 nm to beyond 1100 nm¹. Considering the transmission curve of this *I* + *z* filter, the spectral response curve of the CCD detector, and the spectral type of the target, we derive an effective wavelength ~ 910 nm for the observations. The positions of the stars on the chip were maintained to within a few pixels over the course of each run, thanks to a 'software guiding' system deriving regularly an astrometric solution for the most recently acquired image and sending pointing corrections to the mount if needed.

After a standard pre-reduction (bias, dark, flatfield correction), the stellar fluxes for each run were extracted from the images using the IRAF/DAOPHOT² aperture photometry software (Stetson, 1987). The same photometric aperture of 8 pixels ($\sim 5.1''$) was used for all nights. After a careful selection of stable reference stars of similar brightness, differential photometry was then obtained. Finally, the light curves were normalized. The twelve resulting light curves are shown in Fig. 1. To assess the night-to-night variability of the target, we also extracted a global differential light curve that is shown in Fig. 2.

The typical full-width at half maximum of TRAPPIST point-spread function (PSF) is ~ 3 pixels = $\sim 2''$. At this resolution, the two components of the $1.5''$ binary are only partially resolved (Fig. 3), and our photometry extracted with an aperture of $\sim 5.1''$ radius shows thus the evolution of the sum of the fluxes of both components.

3. Data analysis

While being relatively stable on longer timescales (Fig. 2), Luhman 16 shows a clear variability on a nightly timescale (Fig. 1). Furthermore, the observed patterns evolve strongly

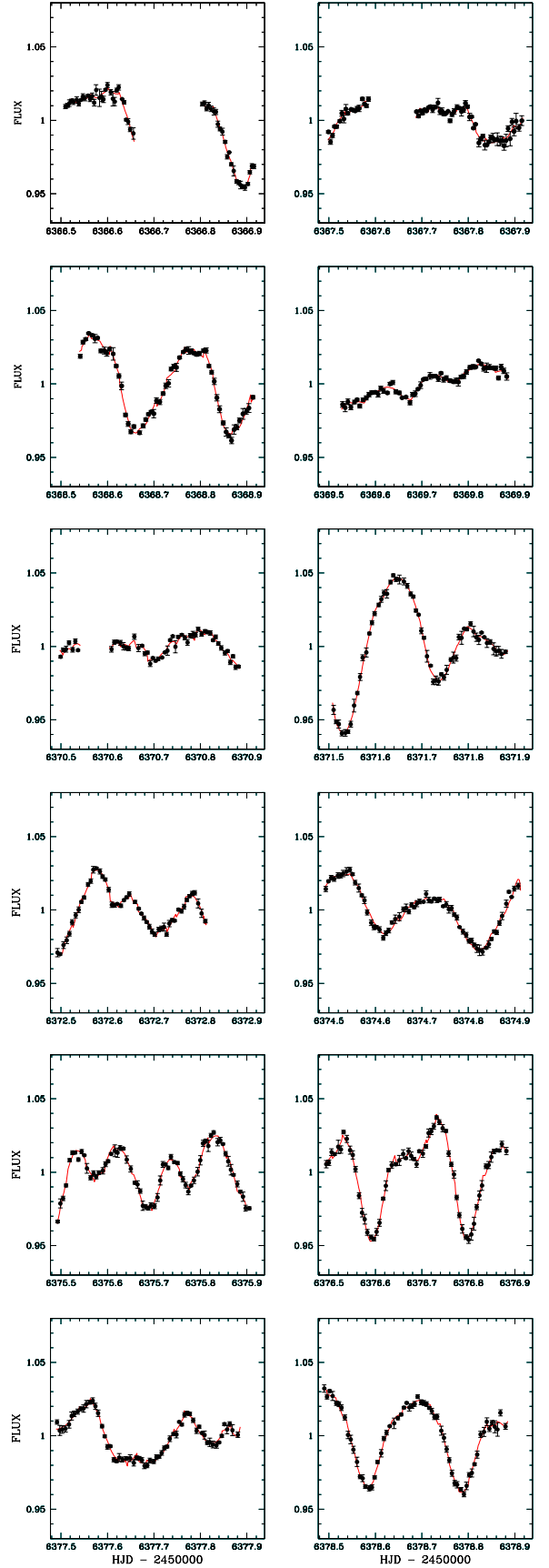


Fig. 1. Normalized TRAPPIST light curves for Luhman 16 binned per 10min intervals. For each light curve, the best-fit global model (see Sec. 3) is over-imposed in red. Gaps for night #1 and #5 correspond to cloudy conditions. The gap for night #2 corresponds to the observation of another target.

¹ <http://www.astrodon.com/products/filters/near-infrared/>

² IRAF is distributed by the National Optical Astronomy Observatory, which is operated by the Association of Universities for Research in Astronomy, Inc., under cooperative agreement with the National Science Foundation.

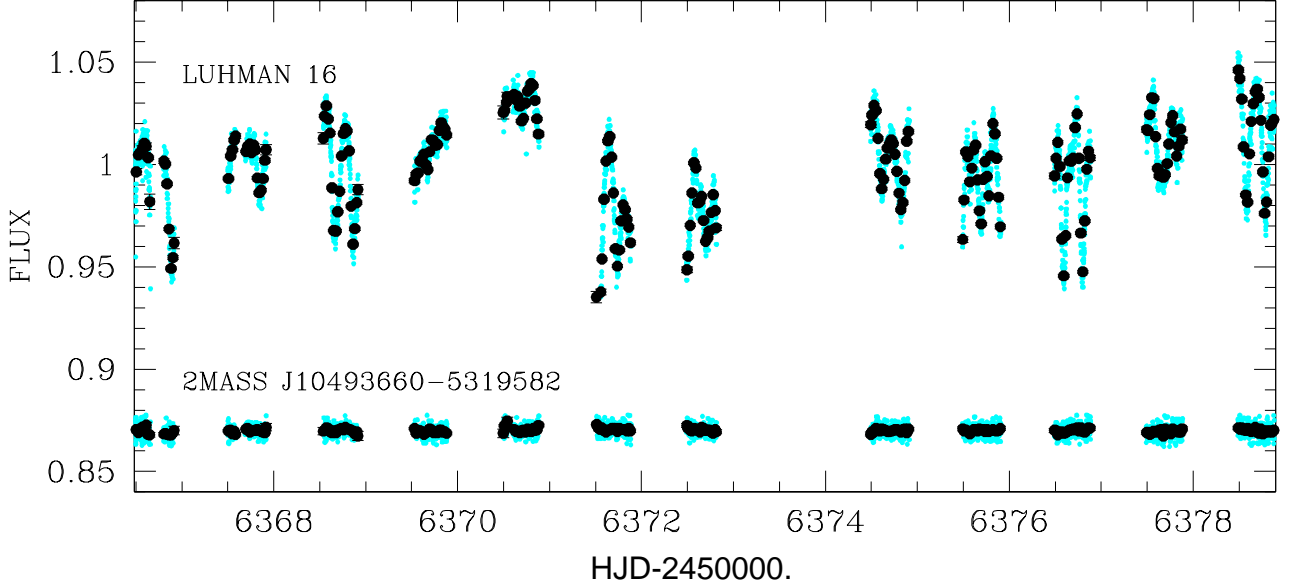


Fig. 2. Globally normalized TRAPPIST differential photometry for Luhman 16 (*top*) and for one of the comparison stars used in the reduction (*bottom*, shifted along the y-axis for the sake of clarity), unbinned (*cyan*) and binned per interval of 30min (*black*). The standard deviation of the binned light curves are 2.2% and 0.1% for Luhman 16 and the comparison star, respectively.

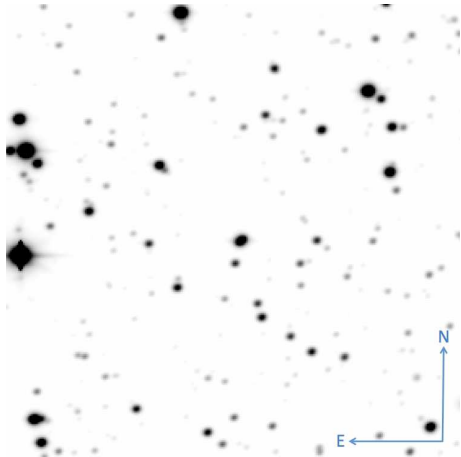


Fig. 3. 3'×3' sub-part centered on Luhman 16 of the combination of the 2783 TRAPPIST images.

from one night to the other. A Lomb-Scargle periodogram (Lomb 1976; Scargle 1982) applied to our photometry shows a strong power excess around ~ 0.2 d (Fig. 4), matching well the typical separation between similar features in the light curves.

We performed a global analysis of our twelve light curves, adapting for that purpose the Markov Chain Monte Carlo (MCMC) code described in Gillon et al. (2012, hereafter G12). In a first step, we assumed that the observed variability was originating from only one of the two BDs. Our basic model for the rotational modulation was based on a division of the brown dwarf into 10 longitudinal slices. For each of them, the surface flux was assumed to be constant during each night, the measured flux being modeled by a semi-sinusoidal function falling to zero when the slice disappears from view. To this rotational model, we added a baseline model accounting for (i) the flip of the equatorial mount of the telescope at the meridian, putting the stellar images on different pixels and thus possibly creating small offsets

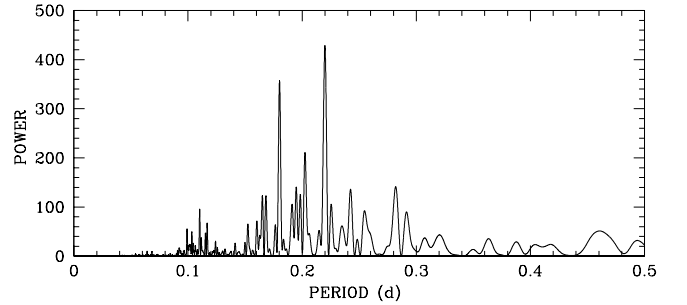


Fig. 4. Lomb-Scargle periodogram for the TRAPPIST photometry of Luhman 16. The peak at ~ 0.18 d is the alias of the stronger peak at ~ 0.22 d.

in the differential photometry, (ii) a 2nd-order airmass polynomial aiming to model the differential extinction curvature due to the much redder color of the target compared to the comparison stars, and (iii) a 4th-order time polynomial representing the low-frequency variability of the system, including the evolution of the patterns from one rotation to the other. In this global model, the only two perturbed parameters in the MCMC were the rotation period and an arbitrary phase, the solution for the remaining parameters being obtained by linear regression at each step of the Markov chains (see G12 for details). Two MCMC chains of 100,000 steps were performed to probe efficiently the posterior distribution of the rotational period.

At the end, we obtain $P_{rot} = 4.87 \pm 0.01$ h, with an excellent fit between the model and the data (see Fig. 1). A Lomb-Scargle periodogram of the residual light curves did not reveal any significant power excess. Nevertheless, we performed a second global MCMC analysis, adding another rotational model to the global model. This analysis failed to identify a second period, while the resulting Bayesian Information Criterion (BIC, Schwarz 1978) was significantly increased (+360), indicating that a model in-

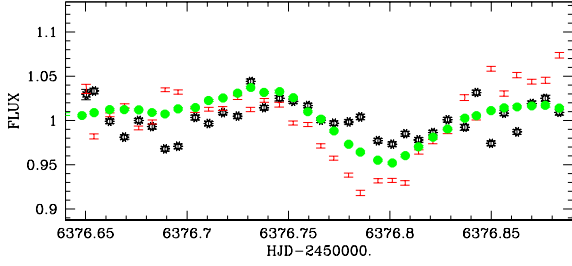


Fig. 5. Differential photometry for the second part of night #10, obtained with an aperture encompassing both components of the binary (*filled green circles*), and with apertures encompassing only the PSF center of Luhman 16A (*black empty symbols*) and Luhman 16B (*red vertical bars*). The amplitude of the variations is amplified on Luhman 16B, indicating that they originate from this T-dwarf.

cluding a single rotation period is a more likely representation of the data. We thus conclude that the one of the two BDs dominates the photometric variability of the binary in the near-IR, the same rotational period for both BDs seeming very unlikely.

Aiming to determine which of the two BDs is the source of the observed variability, we performed a new photometric reduction of a fraction of our images with the TRAF/DAOPHOT ALLSTAR PSF-fitting software (Stetson 1987). But because of the spatial variability of the PSF in TRAPPIST images, we could not unambiguously determine from which BD was originating the signal. Still, this analysis allowed us to determine that the B component is 1.1 ± 0.1 brighter than the A component, corresponding to $\Delta\text{mag} = -0.1 \pm 0.1$. At this stage, we tried another approach to determine the origin of the signal. Using only partial light curves corresponding to both the largest signal amplitude and to the smallest and most stable PSF widths, we extracted the fluxes of both components by aperture photometry, fixing the apertures centers for the two BDs to two opposite positions on the line connecting their PSF centers, on each side of the binary. The aperture sizes were then chosen to encompass only one PSF center. For some light curves, the results were ambiguous, but for several light curves, a signal similar to the one shown in Fig. 1 but with a larger amplitude was visible for the T-dwarf, while no light curve obtained for the L-dwarf showed any significant signal. This is illustrated for a fraction of night #10 in Fig. 5. From these results, we conclude that the detected quasi-periodic variability originates from the T-dwarf Luhman 16B.

4. Discussion

From their new spectroscopy and from the relationship of Stephens et al. (2009), K13 attribute to Luhman 16A and B components effective temperatures of $1350 \pm 120\text{K}$ and $1220 \pm 110\text{K}$, respectively. Such very low temperatures make atmospheric condensates the most likely source of the observed rotational variability (see discussion by Radigan et al. 2012 for the T1.5 BD 2M2139). The most surprising feature of the patterns reported here is their fast evolution from night to night. To our knowledge, this is the first time that such rapid evolution is reported for the cloud coverage of an L/T transition BD, making Luhman 16B an actual ‘Rosetta Stone’ for the study of BDs atmospheres. Future multi-band and high-cadence spectroscopic time-series will be able to observe while clouds condensate and are then dis-

persed, giving unprecedented access into the physico-chemical processes acting in such atmospheres.

Considering our measured $\Delta\text{mag} = 0.1 \pm 0.1$ between both BDs, the variability amplitudes visible in Fig. 1 are thus diluted by a factor ~ 2 by the blend of both PSFs in the TRAPPIST images. The actual maximal peak-to-peak variability amplitude of Luhman 16B should thus be $>20\%$. Similar amplitudes were observed around $1\mu\text{m}$ for at least another early T-dwarf, the T1.5-type BD 2M2139 (Radigan et al. 2012). For the L-dwarf Luhman 16A, we do not detect any variability, but our sensitivity is limited by the partial resolution of both components in our images. High-cadence photometry with a better spatial resolution will be needed to thoroughly assess its photometric variability.

Binary stars have been used from the dawn of modern astronomy as a means to control some variables, while leaving others free. In our case both BDs probably formed together out of the same fragment; they should have their age and composition on a par. What differentiates them is their mass. This affects their respective effective temperatures and densities. Although only 100 K apart, that one shows clouds breaking while the other does not is an indication of how sharp the boundary from a stable to an unstable atmosphere is, and of how closely tuned it must be to effective temperature and scale height.

Field BDs are very interesting targets for exoplanets transit searches (Blake et al. 2008; Bolmont et al. 2011; Belu et al. 2013), as their small sizes make possible the detection of terrestrial planets with photometric precisions at the mmag level similar to the ones reported here for Luhman 16. A careful visual inspection of the residuals light curves and a search for periodic box-like patterns with the BLS algorithm (Kovacs et al. 2002) failed to detect any transit-like signal. Despite the blend of both BDs, our sensitivity is good enough to partially probe the terrestrial regime. Fig. 6 (top panel) shows the residuals of our global modeling compared to the expected transit depths for a $2 R_{\oplus}$ radius planet, for both BDs, assuming for each of them a $0.1 R_{\oplus}$ radius. The corresponding transit is firmly discarded by our data. For orbital periods smaller than the mean duration of our runs ($\sim 9.5\text{h}$), our detection threshold goes down to Earth-size planets, as can be seen in Fig. 6 (bottom panel). This shows that intensive campaigns like the one described here targeting the most nearby field BDs with small to medium-sized ground-based telescopes or, better, with an infrared space facility like *Spitzer* (Triaud et al. in prep.) could efficiently assess the frequency of close-in terrestrial planets around BDs, possibly detecting Earth-sized planets amenable for atmospheric characterization with, e.g., JWST (Belu et al. 2013).

Acknowledgements. TRAPPIST is a project funded by the Belgian Fund for Scientific Research (Fonds National de la Recherche Scientifique, F.R.S-FNRS) under grant FRFC 2.5.594.09.F, with the participation of the Swiss National Science Foundation (SNF). M. Gillon and E. Jehin are FNRS Research Associates. A.H. M. J. Triaud is Swiss National Science Foundation fellow under the grant PBGEP2-145594. C. Opitom and L. Delrez thank the Belgian FNRS for funding their PhD theses.

References

- Artigau, E., Bouchard, S., Doyon, R., Lafrenière, D. 2009, *ApJ*, 701, 1534
- Apai, D., Radigan, J., Buenzli, E., et al. 2013, *ApJ* (in press), arXiv:1303.4151
- Belu, A. R., Selsis, F., Raymond, S. N., et al. 2013, *ApJ* (in press), arXiv:1301.4453
- Bolmont, E., Raymond, S. N., Leconte, J. 2011, *A&A*, 535, 94
- Blake, C. H., Bloom, J. S., Latham, D. W., et al. 2008, *PASP*, 120, 860
- Burgasser, A. J., Marley, M. S., Ackerman, A. S., et al. 2002, *ApJ*, 571, 151
- Burgasser, A. J., Sheppard, S. S., & Luhman, K. L. 2013, *ApJ* (submitted), arXiv:1303.7283

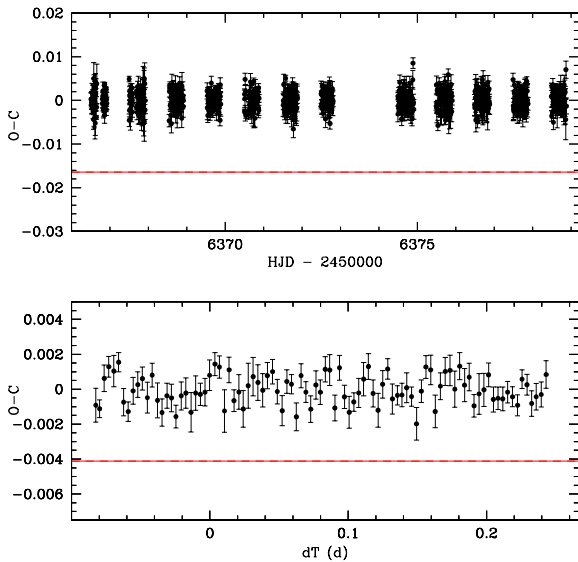


Fig. 6. Residuals of our global modeling, unfolded and binned per 10min intervals (*top*), folded with $P = 8\text{h}$ and binned per 5min intervals (*bottom*). For the unfolded residuals is shown as a red horizontal line the expected transit depth for a $2R_{\oplus}$ planet orbiting one of the two BD, assuming a $0.1R_{\odot}$ radius and the same brightness for both BDs. The same is done for the folded residuals, but assuming a $1R_{\oplus}$ planet.

- Clarke, F. J., Hodgkin, S. T., Oppenheimer, B. R., et al. 2008, MNRAS, 386, 2009
- Gillon, M., Jehin, E., Magain, P., et al. 2011, *Detection and Dynamics of Transiting Exoplanets*, Proceedings of OHP Colloquium (23-27 August 2010), eds. F. Bouchy, R. F. Diaz & C. Moutou, Platypus Press, 06002
- Gillon M., Triaud A. H. M. J., Fortney J. J., et al. 2012, A&A, 542, 4
- Herbst, W., Eisloffel, J., Mundt, R., & Scholz, A. 2007, *Protostars and Planets V*, B. Reipurth, D. Jewitt, and K. Keil (eds.), University of Arizona Press, Tucson, 951, 297
- Khandrika, H., Burgasser, A. J., Melis, C., et al. 2013, AJ, 145, 71
- Kovacs, G., Zucker, S., & Mazeh, T. 2002, A&A, 391, 369
- Jehin, E., Gillon, M., Queloz, D., et al. 2011, The Messenger, 145, 2
- Kirkpatrick, J. D. 2005, ARA&A, 43, 195
- Kniazev, A. Y., Vaisanen, P., Muzic, K., et al., 2013, ApJL (submitted), arXiv1303.7171
- Lomb, N. R., 1976, Ap&SS, 39, 447
- Luhman, K. L. 2013, ApJL (in press), arXiv:1303.2401
- Mamajek, E. E. 2013, arXiv1303.5345
- Mayor, M., & Queloz D. 1995, Nature, 378, 355
- Rebolo, R., Zapatero Osorio, M. R., & Martín, E. L. 1995, Nature, 377, 129
- Radigan, J., Jayawardhana, R., Lafrenière, D., et al. 2012, ApJ, 750, 105
- Saumon, D., & Marley, M. S. 2008, ApJ, 689, 1327
- Scargle, J. D., 1982, ApJ, 263, 835
- Schwarz, G. E. 1978, Annals of Statistics, 6, 461
- Seager, S., & Deming, D. 2010, Exoplanets Atmospheres, ARAA, 48, 631
- Showman, A. P., & Kaspi, Y. 2012, ApJ (submitted), arXiv:1210.7573
- Stephens, D. C., Leggett, S. K., Cushing, M. C., et al. 2009, ApJ, 702, 154
- Stetson, P. B. 1987, PASP, 99, 111
- Vrba, F. J., Henden, A. A., Luginbuhl, C. B., et al. 2004, AJ, 127, 2948